Inorganic Chemistry

Article

pubs.acs.org/IC

Hydrothermal Synthesis, Crystal Structure, and Catalytic Potential of a One-Dimensional Molybdenum Oxide/Bipyridinedicarboxylate Hybrid

Tatiana R. Amarante,[†] Patrícia Neves,[†] Anabela A. Valente,[†] Filipe A. Almeida Paz,*[,†] Andrew N. Fitch,[‡] Martyn Pillinger,[†] and Isabel S. Gonçalves*[,†]

[†] Department of Chemistry, CICECO, University of Aveiro, Campus Universitário de Santiago, 3810-193 Aveiro, Portugal

[‡] European Synchrotron Radiation Facility, B.P. 220, F-38043 Grenoble, France

Supporting Information

ABSTRACT: The reaction of MoO_3, 2,2′-bipyridine-5,5-dicarboxylic acid (H_2bpdc), water, and dimethylformamide in the mole ratio 1:1:1730:130 at 150 °C for 3 days in a rotating Teflon-lined digestion bomb leads to the isolation of the molybdenum oxide/bipyridinedicarboxylate hybrid material (DMA)[MoO_3(Hbpdc)]·$n$$H_2O$ (**1**) (DMA = dimethylammonium). Compound **1** was characterized by scanning electron microscopy, FT-IR and $^{13}C\{^1H\}$ CP MAS NMR spectroscopies, and elemental and thermogravimetric analyses. The solid state structure of **1** was solved and refined through Rietveld analysis of high resolution synchrotron X-ray powder diffraction data in conjunction with information derived from the above techniques. The material, crystallizing in the noncentrosymmetric monoclinic space group *Pc*, is composed of an anionic one-dimensional organic−inorganic hybrid polymer, $_\infty^1$[MoO_3(Hbpdc)]$^-$, formed by corner-sharing distorted {MoO_4N_2} octahedra, which cocrystallizes with charge-balancing DMA^+ cations and one water molecule per metal center. In the crystal structure of **1**, the close packing of individual anionic polymers, DMA^+ cations, and water molecules is mediated by a series of supramolecular contacts, namely strong (O−H···O, N^+−H···O^-) and weak (C−H···O) hydrogen bonding interactions, and π−π contacts involving adjacent coordinated $Hbpdc^-$ ligands. The catalytic potential of **1** was investigated in the epoxidation reactions of the bioderived olefins methyl oleate (Ole) and DL-limonene (Lim) using *tert*-butylhydroperoxide (TBHP) as the oxygen donor and 1,2-dichloroethane (DCE) or (trifluoromethyl)benzene (BTF) as cosolvent, at 55 or 75 °C. Under these conditions, **1** acts as a source of active soluble species, leading to epoxide yields of up to 98% for methyl 9,10-epoxystearate (BTF, 75 °C, 100% conversion of Ole) and 89% for 1,2-epoxy-*p*-menth-8-ene (DCE, 55 °C, 95% conversion of Lim). Catalytic systems employing the ionic liquid 1-butyl-3-methylimidazolium bis(trifluoromethylsulfonyl)imide as solvent could be effectively recycled.

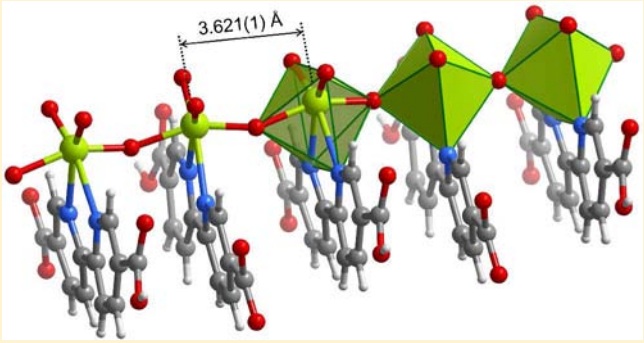

INTRODUCTION

Molybdenum oxide-based organic−inorganic hybrid materials have been of interest for several years due to their potential application in important fields such as catalysis, sorption, electrical conductivity, magnetism, electronics, and optical materials.[1,2] By using the organic component to alter the inorganic oxide microstructure, a very large family of materials has been prepared with structures that comprise one-dimensional (1D) chains, 2D sheets, and 3D networks, as well as discrete clusters. One class of materials that has attracted particular attention is that in which the organic component is an organonitrogen compound. For convenience of classification, these materials have been divided into three subclasses based on the role of the organic molecule as (1) a charge-compensating organoammonium cation, (2) a ligand bonded to a secondary transition-metal cation, and (3) a ligand bonded directly to a molybdenum site of the oxide substructure.[1] Some examples of the ligands used are 2,2′-bipyridine (2,2′-bipy),[2a−c] 4,4′-bipyridine,[2d−f] 2,2′-dipyridylamine,[2g] 4,4′-dipyridylamine,[2h,i] 1,10-phenanthroline,[2j] 2-(1*H*-pyrazol-3-yl)pyridine (pzpy),[2k] pyrazine,[2l] 2,4,6-tripyridyltriazine,[2m] 1,2,3-triazole,[2n] and 1,2,4-triazoles.[2o]

The conventional preparation of oxomolybdenum hybrids belonging to subclass 3 involves the hydrothermal treatment at 160−200 °C of aqueous solutions containing the organic molecule and the molybdenum source, which is typically Na_2MoO_4, MoO_3, or $(NH_4)_6Mo_7O_{24}$. This method frequently affords crystals suitable for X-ray diffraction. Alternative soft chemistry routes include oxidative decarbonylation of molybdenum carbonyl complexes[3] and hydrolysis of dichlorodioxomolybdenum(VI) complexes.[4] For example,

Received: January 31, 2013
Published: March 26, 2013

   dx.doi.org/10.1021/ic400248m | *Inorg. Chem.* 2013, 52, 4618−4628

reaction of $Mo(CO)_4$(2,2′-bipy) with *tert*-butylhydroperoxide gives $[MoO_3$(2,2′-bipy)] with a structure comprising 1D chains of corner-sharing distorted $\{MoO_4N_2\}$ octahedra,[3a] while reaction of MoO_2Cl_2(2,2′-bipy) with water gives $\{[MoO_3$(2,2′-bipy)$][MoO_3(H_2O)]\}_n$ with a structure containing 1D inorganic and organic−inorganic polymers linked by O−H···O hydrogen bonds.[4a] Performing the above two reactions using the ligand 4,4′-di-*tert*-butyl-2,2′-bipyridine (di-*t*Bu-bipy) resulted in the isolation of the octanuclear complexes $[Mo_8O_{24}$(di-*t*Bu-bipy)$_4]$ and $[Mo_8O_{22}(OH)_4$(di-*t*Bu-bipy)$_4]$ from $Mo(CO)_4$(di-*t*Bu-bipy) and MoO_2Cl_2(di-*t*Bu-bipy), respectively.[3a,4b]

The molybdenum oxide/bipy hybrids are active, selective, and stable catalysts for the epoxidation of nonfunctionalized olefins, ranging from the model substrate *cis*-cyclooctene to more demanding substrates of industrial importance such as biorenewable olefins.[3,4] The catalytic application of $\{[MoO_3$(2,2′-bipy)$][MoO_3(H_2O)]\}_n$ was successfully extended to the oxidation of secondary amines to nitrones under mild reaction conditions.[5]

Motivated by the promising catalytic properties of molybdenum oxide/bipy hybrids, we set out to extend the structural complexity of this family of materials by using another variant to the ligand 2,2′-bipy, namely 2,2′-bipyridine-5,5-dicarboxylic acid (H_2bpdc). The choice of this ligand was partly based on the bifunctionality of its deprotonated form (bpdc), which makes it an attractive connector ligand for the synthesis of metal organic frameworks.[6] Hydrothermal reaction of MoO_3 in the presence of H_2bpdc and dimethylformamide (DMF) yields (DMA)$[MoO_3$(Hbpdc)$]\cdot nH_2O$ (**1**) (DMA = dimethylammonium), which has been fully characterized by various techniques and represents the first material of its type incorporating an anionic 1D hybrid polymer. Catalytic studies reveal that **1** promotes the epoxidation of biorenewable olefins, specifically DL-(+)-limonene and methyl oleate, to the corresponding epoxides.

EXPERIMENTAL SECTION

Materials and Methods. MoO_3 (99.5%, AnalaR), 2,2′-bipyridine-5,5′-dicarboxylic acid (Sigma-Aldrich), DMF (puriss p.a., Sigma-Aldrich), methyl oleate (Ole, 99%, Aldrich), and 5−6 M *tert*-butylhydroperoxide (TBHP) in decane (Aldrich) were acquired from commercial sources and used as received. DL-Limonene (Lim, ≥95%, Merck) was dried prior to use by using activated 4 Å molecular sieves. For catalysis, 1,2-dichloroethane (DCE, 99%, Aldrich) and (trifluoromethyl)benzene (BTF, anhydrous, 99%, Aldrich) were dried prior to use by stirring over CaH_2 overnight, followed by distillation, and storage over activated 4 Å molecular sieves. The ionic liquids (ILs) 1-butyl-3-methylimidazolium tetrafluoroborate ([bmim]-BF_4, Merck, ≥98%), 1-butyl-3-methypyridinium tetrafluoroborate ([bmpy]BF_4, Merck, ≥98%), and 1-butyl-3-methylimidazolium bis-(trifluoromethylsulfonyl)imide ([bmim]NTf_2, IoLiTec, 99%) were predried at 100 °C under vacuum (<0.1 bar) for 2 h.

Elemental analysis for C, H, and N was performed at the University of Aveiro using a Truspec instrument. Routine X-ray powder diffraction (XRPD) data were collected on an X'Pert MPD Phillips diffractometer (Cu Kα X-radiation, λ = 1.54060 Å) fitted with a curved graphite monochromator and a flat plate sample holder, in a Bragg−Brentano para-focusing optics configuration (40 kV, 50 mA). Samples were step-scanned in the range from 3.5 to 70° 2θ with steps of 0.02° and a counting time of 25 s per step. Scanning electron microscopy (SEM) images and energy dispersive X-ray spectroscopy (EDS) data were collected using a Hitachi S4100 scanning electron microscope operating at 25 kV. Samples were prepared by deposition on aluminum sample holders followed by carbon coating using an Emitech K 950 carbon evaporator. Thermogravimetric analyses were performed under air using a Shimadzu TGA-50 system with a heating rate of 5 °C min^{-1}.

FT-IR spectra were collected using KBr (Aldrich 99%, FT-IR grade) pellets on a Mattson-7000 infrared spectrophotometer. FT-Raman spectra (range 100−4000 cm^{-1}) were recorded on a Bruker RFS 100 spectrometer with a Nd:YAG coherent laser (λ = 1064 nm). Solid state ^{13}C cross-polarization (CP) magic-angle-spinning (MAS) NMR spectra were recorded using a Bruker Avance 400 spectrometer (9.4 T) at 100.62 MHz with 3.7 μs ^{1}H 90° pulses, 1.5 ms contact time, spinning rates of 11 kHz, and 5 s recycle delays. Chemical shifts are quoted in parts per million (ppm) from tetramethylsilane.

Synthesis of (DMA)$[MoO_3$(Hbpdc)$]\cdot nH_2O$ (1). A mixture of MoO_3 (89 mg, 0.62 mmol), 2,2′-bipyridine-5,5′-dicarboxylic acid (151 mg, 0.62 mmol), H_2O (19 mL), and DMF (6 mL) was heated in a rotating (10 rpm) Teflon-lined digestion bomb at 150 °C for 3 days. After cooling to room temperature, the orange solution (pH = 6) was transferred to a Schlenk tube and left to rest for 4 days. A white solid gradually precipitated, which was filtered, washed with water (4 × 10 mL) and diethyl ether (4 × 5 mL), and finally vacuum-dried. Yield: 160 mg, 56%. Anal. Calcd for $C_{14}H_{18.4}MoN_3O_{8.7}$ (n = 1.7): C, 36.25; H, 4.00; N, 9.06. Found: C, 36.37; H, 3.71; N, 9.02. FT-IR (KBr, cm^{-1}): ν = 3442 (s), 3214 (m), 3106 (m), 3086 (m), 3040 (m), 2978 (w), 2787 (s), 2439 (w), 1725 (s), 1648 (s), 1602 (s), 1578 (m), 1565 (m), 1497 (w), 1470 (m), 1364 (s), 1293 (s), 1278 (s), 1261 (s), 1144 (m), 1130 (m), 1022 (m), 967 (w), 922 (vs), 901 (vs), 860 (m), 819 (vs), 770 (vs), 745 (w), 727 (m), 692 (s), 646 (sh), 576 (vs, br), 448 (s), 411 (s), 350 (w), 324 (w). FT-Raman (cm^{-1}): ν = 3086 (m), 3040 (w), 2975 (w), 1598 (vs), 1496 (w), 1406 (w), 1359 (w), 1316 (s), 1286 (m), 1260 (w), 1141 (w), 921 (vs), 858 (m), 803 (w), 768 (w), 646 (w), 573 (w), 443 (w), 410 (w), 326 (w), 226 (m), 207 (m), 132 (s). ^{13}C MAS NMR: δ = 169.0 and 168.0 (COOH, CO_2^-), 150.0, 148.5, 146.4, 142.4, 139.4, 130.2, 123.4 (all bipy-C), 36.1 (CH_3) ppm.

Synchrotron XRPD Studies. High-resolution synchrotron XRPD data suitable for crystal solution were collected at 100 K on the powder diffractometer at the ID31 beamline of the European Synchrotron Radiation Facility (ESRF), Grenoble, France. Table 1 gathers all the details pertaining to the synchrotron X-ray data collection, crystal data, and structure refinement (profile and reliability factors) for (DMA)$[MoO_3$(Hbpdc)$]\cdot H_2O$ (**1**). The corresponding final Rietveld plot is supplied in Figure 1. A complete description of the procedures used is given in the Supporting Information. Structural drawings were created using the software package Crystal Impact Diamond.[7] Crystallographic data (excluding structure factors) for **1** have been deposited with the Cambridge Crystallographic Data Centre as No. 917846. Copies of the data can be obtained free of charge via the Internet at http://www.ccdc.cam.ac.uk/conts/retrieving.html or by post at CCDC, 12 Union Road, Cambridge CB2 1EZ, U.K. (fax: 44-1223336033, e-mail: deposit@ccdc.cam.ac.uk).

Catalysis. The epoxidation reactions were carried out in 5 mL borosilicate microreactors at a stirring rate of 1000 rpm under autogenous pressure. The microreactors containing the olefin/**1**/cosolvent were immersed in the thermostated oil bath and preheated to the desired reaction temperature (55 or 75 °C) for 10 min prior to addition of oxidant solution, which was preheated in a similar fashion; the addition of the oxidant was taken as the initial instant of the catalytic reaction. Initial molar ratios of Mo/olefin/TBHP were typically 1:103:160 (17 μmol of molybdenum per catalytic test). DCE or BTF (1 mL), or IL (0.3 mL), was added as cosolvent.

The evolutions of the catalytic reactions were monitored using a Varian 3900 GC equipped with a FID detector and a capillary column (J&W Scientific DB-5, 30 m × 0.25 mm × 0.25 μm) and using undecane or methyl decanoate as internal standards. Reaction products were identified by GC-MS (Trace GC 2000 Series Thermo Quest CE Instruments GC; Thermo Scientific DSQ II) with He as carrier gas.

To assess the homo-/heterogeneous nature of the catalytic reaction for the system **1**/olefin/BTF/75 °C, a catalytic test (denoted CatFilt) was carried out as follows: after 2 h the hot reaction mixture was filtered through a 0.2 μm PTFE membrane filter, and the filtrate was

dx.doi.org/10.1021/ic400248m | Inorg. Chem. 2013, 52, 4618−4628

Table 1. X-ray Data Collection, Crystal Data, and Structure Refinement Details for (DMA)[MoO_3(Hbpdc)]·H_2O (1)

Data Collection		
diffractometer	ID31 beamline—ESRF, France	
wavelength/Å	0.39981(1)	
temp/K	100	
geometry	Debye–Scherrer	
2θ range (deg)	1.012–30.000	
step size (deg)	0.002	
Unit Cell		
formula	$C_{14}H_{17}MoN_3O_8$[a]	
formula weight	451.25[a]	
crystal system	monoclinic	
space group	*Pc*	
a/Å	8.40330(4)	
b/Å	13.69246(6)	
c/Å	7.24076(2)	
β/deg	100.5825(4)	
volume/Å^3	818.965(6)	
Z	2	
D_c/(g cm^{-3})	1.830[a]	
Profile Parameters		
profile function	Thompson–Cox–Hastings pseudo-Voigt	
overall temperature factor	0.81(3) Å^2	
profile parameters	*U* = 0.041(1)	*X* = 0.0067(1)
	V = −0.00221(8)	*Y* = 0.00235(8)
	W = 0.00006(1)	
asymmetry parameters (up to 5° 2θ)	0.0094(3) and 0.0049(1)	
zero shift (2θ°)	0.002(1)	
Refinement Details		
no. of independent reflections	1904	
no. of global refined parameters	1	
no. of profile refined parameters	13	
no. of intensity-dependent refined parameters	123	
Reliability Factors for Data Points with Bragg Contribution (Conventional—Not Corrected for Background)		
R_p, R_{wp}, R_{exp}, χ^2	8.86, 12.6, 4.98, 6.42	
Structure Reliability Factors		
R_{Bragg}, R_F	9.32, 11.3	

[a]Hydrogen atoms associated with the water molecule of crystallization have been added to the empirical formula and used in the calculation of the related structural parameters.

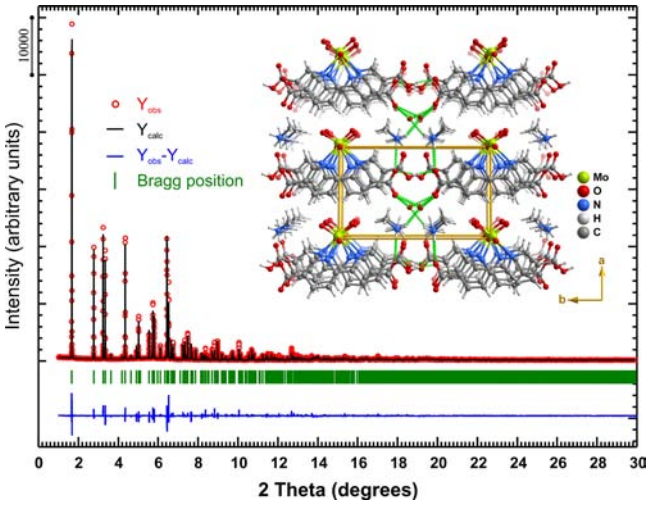

Figure 1. Final Rietveld plot (synchrotron XRPD data) of (DMA)-[MoO_3(Hbpdc)]·H_2O (**1**). Observed data points are indicated as red circles, and the best fit profile (upper trace) and the difference pattern (lower trace) are drawn as solid black and blue lines, respectively. Green vertical bars indicate the angular positions of the allowed Bragg reflections. Refinement details are given in Table 1. A ball-and-stick crystal packing representation of **1** viewed down the [001] crystallographic direction is provided as an inset.

RESULTS AND DISCUSSION

Synthesis. Hydrothermal reaction of MoO_3 and 2,2′-bipyridine-5,5-dicarboxylic acid (H_2bpdc) in a mixture of water and DMF at 150 °C for 3 days gave a clear orange solution. After cooling to room temperature, the title compound, (DMA)[MoO_3(Hbpdc)]·*n*H_2O (**1**) (DMA = dimethylammonium), began to precipitate from the solution and was eventually isolated in 56% yield (*n* = 1.7) after allowing the reaction mixture to stand at room temperature for 4 days. The use of DMF as cosolvent is necessary to promote dissolution of H_2bpdc; when the reaction was performed without DMF, only the starting materials were recovered after hydrothermal reaction under the same conditions.

SEM images were obtained to determine crystallite size and morphology (Figure 2). Compound **1** consists of thin slablike crystallites up to at least 12 μm in length. The rectangular shape of the flat plates indicates a preferential growth direction, which is in accordance with the proposed structural model of parallel

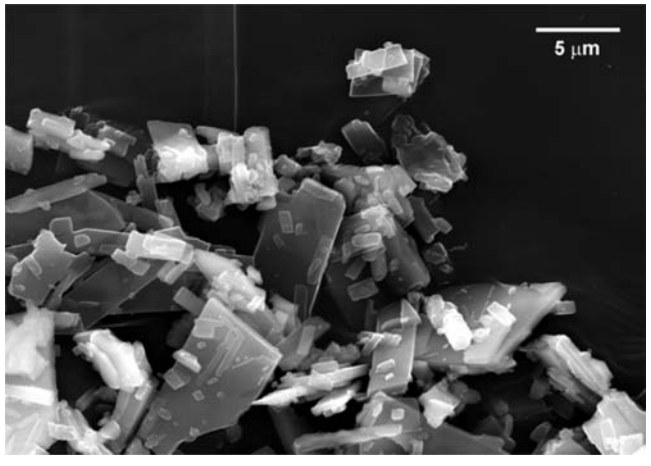

Figure 2. Representative SEM image of **1**.

transferred to a separate microreactor (walls preheated at the reaction temperature), and the reaction solution was stirred and monitored for a further 22 h at 75 °C. The catalytic reaction is considered to be homogeneous in nature when ΔFilt/Δcat ≅ 1, where ΔFilt is the increment in olefin conversion in the time interval 2–24 h for the reaction carried out using the filtered solution and Δcat is the increment in olefin conversion during the same time interval for the reaction carried out in the presence of **1** (i.e., no filtration step).

In order to recycle the IL-based catalytic systems after a 24 h batch run, the reaction products were separated by solvent extraction using *n*-hexane (three extraction cycles using 1.5 mL solvent in each). Subsequently, the catalyst/IL mixture was heated at 40 °C for 1 h under vacuum in order to remove dissolved volatile organic compounds; the absence of extracting solvent and reaction products in the recovered catalyst/IL mixture was confirmed by GC. A second batch run was initiated by adding the reagents to the recovered catalyst/IL mixture in the same amounts as those used in the first batch run.

dx.doi.org/10.1021/ic400248m | Inorg. Chem. 2013, 52, 4618–4628

1-dimensiomal (1D) chains along the crystal *c*-axis (see below). Indeed, under the electron beam of the SEM studies, a unidirectional fragmentation occurred, which likely results from the release of water molecules located between each layer of the 1D chains of the polymer $_{\infty}^{1}[MoO_3(Hbpdc)]^-$.

The thermal decomposition of **1** exhibits a 6.6% weight loss between 25 and 210 °C corresponding to the release of 1.7 water molecules per formula unit (Figure S2 in the Supporting Information), which is in agreement with the chemical composition of as-synthesized **1** determined by CHN microanalyses (please see the Experimental Section). In this temperature range there are clearly two overlapping steps: the first weight loss occurring around 100 °C is attributed mainly to the desorption of physisorbed water on the external surface of the crystallites. The second loss up to 210 °C may be attributed to the release of the remaining water molecules of crystallization (according to the crystal structure solution, there is one water molecule of crystallization per formula unit, which corresponds to 4.0% by weight). Between 210 and 470 °C there is a three-step decomposition of the organic components with a total weight loss of ca. 55.0%. In a separate experiment, a sample of **1** was calcined at 500 °C under air and the resultant powder characterized by routine XRPD, which showed the presence of a poorly crystalline MoO_3 phase. The presence of carbon in the material obtained at 500 °C was indicated by the dark color of the solid and the fact that the residual weight at this temperature is ca. 38.3%, which is significantly higher than that expected for the stoichiometric amount of MoO_3 (theoretical, 31%). For temperatures higher than ca. 720 °C, a further weight loss is observed which is attributed to the simultaneous release of the remaining carbon and to sublimation of MoO_3.[8]

The FT-IR spectrum of **1** exhibits strong, sharp bands at 901 and 922 cm^{-1} assigned to ν(Mo═O) from *cis*-$[MoO_2]^{2+}$ units and a broad, intense band at 576 cm^{-1} attributed to ν(Mo−O−Mo) (Figure 3). For comparison, the 1D organic−inorganic hybrid material $[MoO_3(2,2'\text{-bipy})]$ exhibits a similar set of bands at 622, 882, and 914 cm^{-1}.[2a,3a] A strong (and sharp) band at 1602 cm^{-1} (cf. 1598 cm^{-1} in the Raman spectrum) is assigned to a pyridyl ring stretching vibration and is shifted by about 10 cm^{-1} to higher frequency when compared with the corresponding band for the free ligand H_2bpdc. A very broad absorption peaking at 3442 cm^{-1} (ν_{as}(OH)) and a broad band at 1648 cm^{-1} (OH-bending mode) are associated with water molecules of crystallization involved in hydrogen-bonding interactions. The latter band likely overlaps with a $\nu_{as}(CO_2^-)$ vibration from deprotonated carboxylic acid groups; the corresponding $\nu_s(CO_2^-)$ vibration may be the sharp band at 1364 cm^{-1} or a high frequency shoulder on this band at ca. 1380 cm^{-1} (the assignment is uncertain, since H_2bpdc exhibits a medium-intensity band at 1372 cm^{-1}). A broad, medium-intensity band at 1725 cm^{-1} is assigned to ν(C═O) of COOH groups. Several bands in the range 2400−3250 cm^{-1} support the presence of the charge-balancing dimethylammonium cation, formed during the synthesis by hydrolysis of DMF. In particular, the medium-intensity (and broad) bands peaking at about 3214 cm^{-1} and 2787 cm^{-1} can be attributed to $\nu(NH_2^+)$ and $\nu(CH_3)$ stretching modes, respectively.[9] Several overlapping bands in the range 2970−3110 cm^{-1} arise from $\nu(NH_2^+)$, $\nu(CH_3)$, and aromatic ν(C−H) stretching vibrations. The decomposition of DMF under hydrothermal conditions is quite a common occurrence, and there are a number of examples in the literature where the resultant $(CH_3)_2NH_2^+$ is incorporated as a countercation in an anionic coordination network.[10] In our system the hydrolysis of DMF could be metal-catalyzed and/or promoted by acidic conditions during the initial stages of the reaction.

The $^{13}C\{^1H\}$ CP MAS NMR spectrum of **1** displays signals for the COOH and CO_2^- groups at 168 and 169 ppm, the bipyridyl aromatic carbon atoms between 120 and 150 ppm, and the CH_3 groups of dimethylammonium cations at 36.1 ppm (Figure 4). The presence of eight resolved resonances for the bipyridyl carbons shows that the two pyridyl rings are not equivalent, which is in accordance with the structural model determined from synchrotron XRPD data (all 10 carbons are crystallographically distinct) and the deprotonation of one of the carboxylic acid groups. No peak at ca. 162 ppm characteristic of DMF is observed.

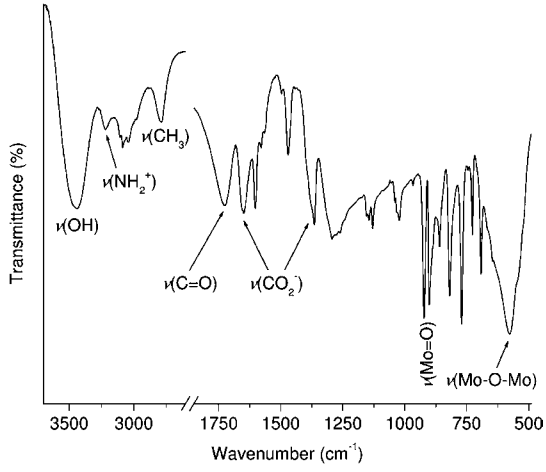

Figure 3. FT-IR spectrum of **1** with selected assignments.

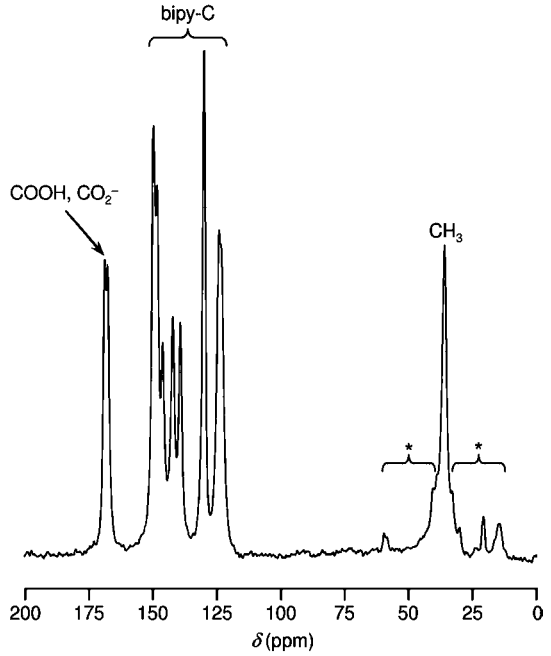

Figure 4. $^{13}C\{^1H\}$ MAS NMR spectrum of **1**. Spinning sidebands are indicated by asterisks (spinning rate = 11 kHz).

dx.doi.org/10.1021/ic400248m | Inorg. Chem. 2013, 52, 4618−4628

Crystal Structure Description and Formation of (DMA)[MoO_3(Hbpdc)]·H_2O. A detailed crystallographic description of **1** was obtained by using *ab initio* methods based on high-resolution synchrotron X-ray powder diffraction data (please see the Supporting Information for details, Figure 1 and Table 1). The material, crystallizing in the noncentrosymmetric monoclinic space group *Pc*, is composed of an anionic one-dimensional (1D) organic−inorganic hybrid polymer, $_\infty^1[MoO_3(Hbpdc)]^-$, which cocrystallizes with charge-balancing DMA^+ cations and one water molecule per metal center.

This novel hybrid material is truly unique. 1D polymers based on dioxomolybdenum units *N*,*N*-chelated by organic ligands, in some cases intercalated by tetrahedral $[MoO_4]^{2-}$ units, have been reported by Zapf et al.[2a] with 2,2′-bipyridine ($_\infty^1[MoO_3(2,2'\text{-bipy})]$ and $_\infty^1[Mo_2O_6(2,2'\text{-bipy})]$), Kim et al. ($_\infty^1[Mo_4O_{12}(2,2'\text{-bipy})_3]$),[2b] and Zhou et al. with 1,10-phenanthroline ($_\infty^1[Mo_3O_9(phen)_2]$).[2j] Nevertheless, in all these materials the hybrid polymers are neutral. The anionic $_\infty^1[MoO_3(Hbpdc)]^-$ polymer reported in this manuscript constitutes, to the best of our knowledge, the first of such polymeric compounds which is negatively charged. Branched cationic polymers having similar environments for the Mo^{6+} centers are known, being crystallographically reported for the first time a few years ago by Li et al.[11] and, more recently, by Dai et al.[12] However, such crystalline architectures could only be achieved by the systematic use of large polyoxometalate anions serving as templates. Furthermore, in these described materials, the 1D chains are not markedly linear, being branched at some point that may also serve as a coordination site for other metals, such as found in the material reported by Li et al.[11]

Despite the crystallization of **1** being slow (i.e., thermodynamically driven), attempts to control this step and isolate crystals suitable for single-crystal X-ray diffraction were unsuccessful. This experimental evidence clearly suggests that nucleation is fast, occurring randomly, while crystal growth is in turn slow and strongly dependent on the self-assembly of the individual building units from solution. Because DMA^+ cations are important in the crystal structure of **1** (details in the following paragraphs), it is reasonable to assume that the formation of this cation from DMF limits in some way the rate of formation of the resultant polymeric material.

The anionic 1D organic−inorganic hybrid polymer, $_\infty^1[MoO_3(Hbpdc)]^-$ (Figure 5a), present in the crystal structure of **1** is formed by a single crystallographically independent Mo^{6+} metal center coordinated to two symmetry-related μ_2-bridging oxido groups (in apical positions), two terminal Mo═O groups, and one *N*,*N*-chelated $Hbpdc^-$ anionic ligand, ultimately describing a highly distorted $\{MoN_2O_4\}$ octahedral coordination environment for which the equatorial plane is composed of the two latter coordinating groups (Figure 5b): while the internal (N,O)−Mo−(N,O) octahedral *trans* angles were found within the equatorial plane and in the 156.9(12)−165.5(13)° range, the *cis* angles are instead in the 68.3(11)−99.8(13)° range; the Mo−(N,O) bond distances range from 1.67(3) to 2.43(3) Å (Table S1 in the Supporting Information). Most of the octahedral distortion arises from within the equatorial plane of the $\{MoN_2O_4\}$ octahedron due to the strong *trans* influence of the two terminal oxido groups with respect to the *N*,*N*-chelated $Hbpdc^-$ anionic ligand. Even though the observed amplitudes for these physical parameters are large, a search in the

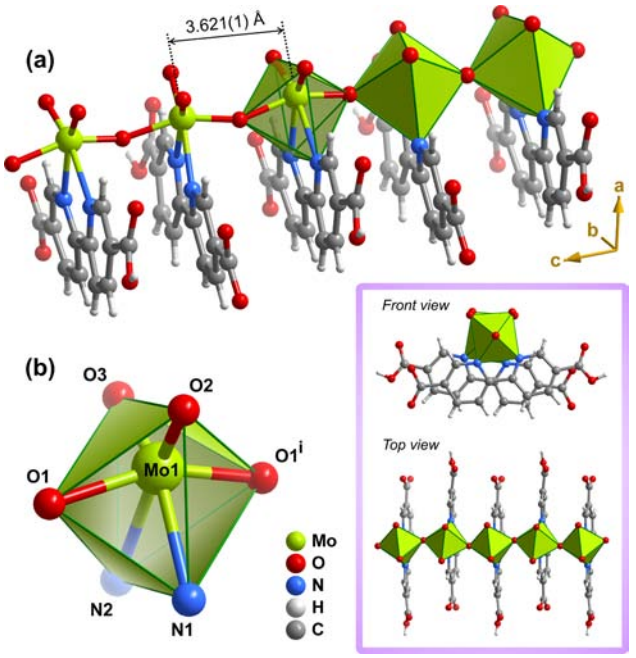

Figure 5. (a) Mixed ball-and-stick and polyhedral representation of the anionic one-dimensional $_\infty^1[MoO_3(Hbpdc)]^-$ hybrid polymer present in **1** running parallel to the [001] direction of the unit cell. (b) Schematic representation of the highly distorted $\{MoN_2O_4\}$ octahedral coordination geometry of Mo1. Selected bond lengths and angles are given in Table S1 in the Supporting Information. Symmetry transformation used to generate equivalent atoms: (i) x, $-y$, $-^1/_2 + z$.

Cambridge Structural Database (CSD, version 5.33 with four updates)[13,14] for the geometrical parameters of $\{MoN_2O_4\}$ octahedra showed that the typical Mo−(N,O) bond distances and (N,O)−Mo−(N,O) angles are found in the *ca.* 1.70−2.37 Å and 72.1−166.1° ranges (median values for each limit; from 188 hits in the database), clearly supporting the chemical feasibility of the structure model derived for compound **1**.

As depicted in Figure 5b, the two symmetry-related μ_2-bridging O1 oxido groups are at the genesis of the 1D $_\infty^1[MoO_3(Hbpdc)]^-$ polymer establishing physical connections between adjacent units. This feature imposes an intermetallic Mo1···$Mo1^i$ separation of 3.621(1) Å (i.e., half of the *c*-axis) and a "kink" Mo1−O1−$Mo1^i$ angle of 154.4(12)° (symmetry transformation: (i) x, $-y$, $-^1/_2 + z$). A search in the literature for similar values in Mo^{6+}-containing polymeric materials reveals that the intermetallic distances are typically found in the 3.66−3.96 Å range (median 3.72 Å), while the "kink" angles of μ_2-bridging oxido groups are instead described in the wide 135.8−175.4° range (median 157.2°). This data clearly shows that while the observed bridging "kink" angle for **1** is rather typical, the intermetallic separation is markedly shorter than in related materials. This structural feature can be rationalized by taking into consideration the various supramolecular contacts mediating the crystal packing of the material and contributing to the overall structural robustness (see further details below).

Within the anionic $_\infty^1[(MoO_3)(Hbpdc)]^-$ polymer, which runs parallel to the *c*-axis of the unit cell, symmetry-related *N*,*N*-chelated $Hbpdc^-$ ligands alternate (concerning the location of the protonated carboxylic acid group) and are slightly tilted with respect to the Mo→O→Mo vector along the polymer (this is particularly notable from a front view of the

dx.doi.org/10.1021/ic400248m | *Inorg. Chem.* 2013, 52, 4618−4628

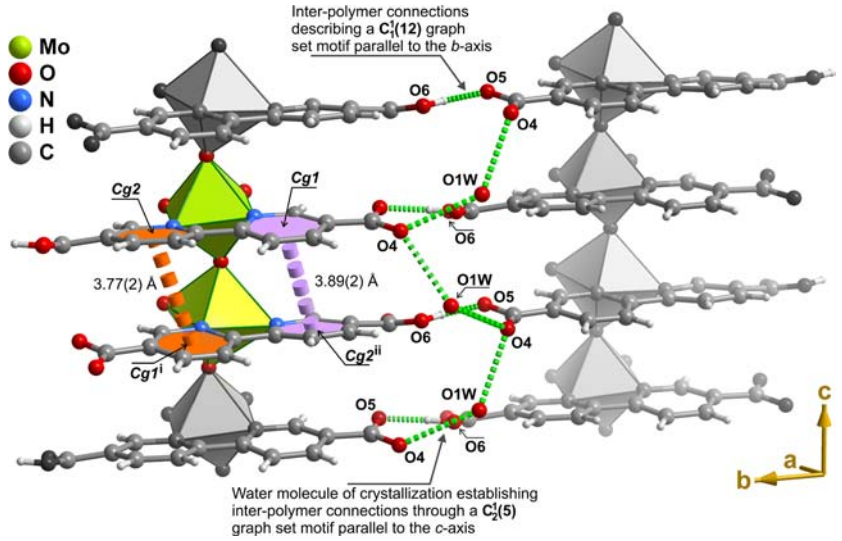

Figure 6. Mixed ball-and-stick and polyhedral representation of the supramolecular contacts (O−H···O hydrogen bonds and $\pi-\pi$ contacts) involving adjacent anionic 1D $_{\infty}^{1}[MoO_3(Hbpdc)]^-$ hybrid polymers in the crystal structure of **1**. For geometrical details on the represented supramolecular contacts, see Table S2 in the Supporting Information. Symmetry transformations used to generate equivalent centroids: (i) x, $-y$, $-^1/_2 + z$; (ii) x, $-y$, $^1/_2 - z$ (please note: transformation operations involving the interpolymer $\mathbf{C}_1^1(12)$ and $\mathbf{C}_2^1(5)$ graph set motifs[15] have been omitted for clarity).

polymer as depicted in Figure 5): the dihedral angle between the two ligands is *ca.* 19.8° for **1**. An analogous dihedral angle of *ca.* 49.6° was previously reported by Zapf et al. for the neutral polymer $_{\infty}^{1}[MoO_3(2,2'\text{-bipy})]$.[2a] The striking difference between these two dihedral angles is attributed mainly to the type of supramolecular interactions mediating the packing of adjacent polymers: while in the anionic polymer reported herein the 5,5′-disubstituted carboxylic acid groups are mutually engaged in strong and highly directional O−H···O hydrogen bonds (Figure 6 and Figure S3 in the Supporting Information), which drive the molecules to be almost aligned along the direction of the polymer, in the close packing of $_{\infty}^{1}[MoO_3(2,2'\text{-bipy})]$, only weak contacts are present, thus allowing the mutual rotation of adjacent 2,2′-bipy molecules so as to minimize steric repulsion. This is also the structural reason why the exact opposite was observed in the material $\{[MoO_3(2,2'\text{-bipy})][MoO_3(H_2O)]\}_n$ previously reported by us:[4a] in this situation the 2,2′-bipy ligands of the neutral $_{\infty}^{1}[MoO_3(2,2'\text{-bipy})]$ polymer are perfectly aligned so as to minimize steric repulsion with the adjacent $_{\infty}^{1}[MoO_3(H_2O)]$.

The close packing of individual anionic $_{\infty}^{1}[MoO_3(Hbpdc)]^-$ polymers, DMA^+ cations, and water molecules of crystallization to yield the crystal structure of **1** is mediated by a series of supramolecular contacts. The most striking interactions concern the strong [$d_{D\cdots A}$ = 2.49(2) Å] and highly directional [$\angle$(DHA) = 169°] O6−H6···O5 hydrogen bonds involving the carboxylic acid groups of adjacent anionic $_{\infty}^{1}[(MoO_3)(Hbpdc)]^-$ polymers, establishing effective physical connection between polymers along the [010] direction of the unit cell and describing an interpolymer $\mathbf{C}_1^1(12)$ graph set motif (Figure 6).[15] Additionally, adjacent coordinated $Hbpdc^-$ ligands interact via offset $\pi-\pi$ contacts, with the intercentroid distances ranging from *ca.* 3.77(2) to 3.89(2) Å. The cooperative effect of both these O−H···O hydrogen bonds and $\pi-\pi$ contacts seems to be the reason why in compound **1** the intermetallic Mo1···Mo1 separation is among the shortest reported to date. Interpolymer connections are also ensured by the water molecule of crystallization which is involved in a $\mathbf{C}_2^1(5)$ graph set motif parallel to the [001] direction, donating the two hydrogen atoms to neighboring carboxylic acid groups (Figures 6 and S3).

The DMA^+ cation is engaged in both strong ($N^+-H\cdots O^-$) and weak (C−H···O) hydrogen bonds, with oxide and carboxylic acid groups belonging to adjacent anionic $_{\infty}^{1}[(MoO_3)(Hbpdc)]^-$ polymers and water molecules of crystallization (Figure S3 and Table S2 in the Supporting Information). The most notable interaction concerns the charged $N^+-H\cdots O^-$ hydrogen bond that this cation establishes with the neighboring carboxylate group, which, despite being relatively long [$d_{D\cdots A}$ = 2.97(4) Å], remains somewhat directional [$\angle$(DHA) = 158°]. The other hydrogen from the protonated $-NH_2^+-$ moiety is in turn donated to the neighboring water molecule. Weak C−H···O hydrogen bonds (see Table S2 for geometrical details) are also present in the crystal structure, connecting not only the DMA^+ cation to adjacent moieties (such as the anionic polymer and water molecules) but also promoting interpolymer connections (the most striking example concerns the C7−H7···O3 interaction—not shown). Despite these supramolecular interactions being of rather weak nature, they are, nevertheless, numerous in the crystal structure of **1**, and in general, they are relatively directional [all $\angle$(DHA) angles are greater than 127°]. Their cooperative effect, alongside the previously described interactions, contributes significantly toward the structural robustness of the material and explains why the self-assembly of the material from solution produces such highly crystalline material.

Catalytic Epoxidation of Olefins. The catalytic performance of **1** was investigated in the epoxidation reactions of the bioderived olefins methyl oleate (Ole) and DL-limonene (Lim) using *tert*-butylhydroperoxide (TBHP) as the oxygen donor and 1,2-dichloroethane (DCE) or (trifluoromethyl)benzene (BTF) as organic cosolvent, at 55 or 75 °C (Scheme 1). Ole is a monounsaturated fatty acid ester present in, for example, methyl oleate soybean oil. Epoxidation of Ole gives methyl 9,10-epoxystearate (OleOx), which is a key intermediate used in the synthesis of several compounds of industrial interest,

dx.doi.org/10.1021/ic400248m | *Inorg. Chem.* 2013, 52, 4618−4628

Scheme 1. Epoxidation Reactions Studied in This Work

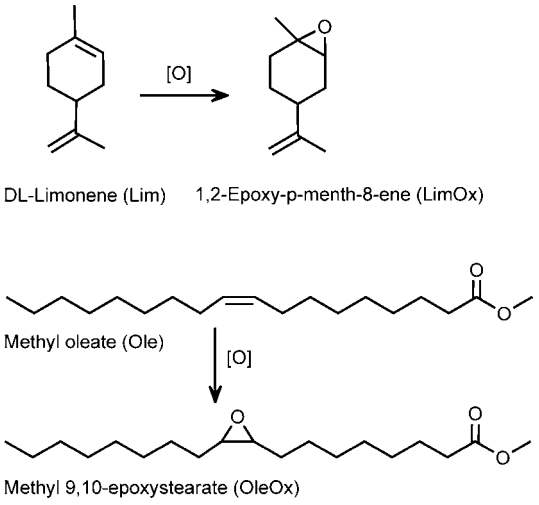

such as polyether polyols,[16] carbonates,[17] and azides.[18] Lim is one of the most common naturally occurring monoterpenes (present in citrus oil), and its epoxidation gives 1,2-epoxy-*p*-menth-8-ene (LimOx), an epoxide monomer with applications that include metal coatings, varnishes, printing inks, and synthesis of biodegradable polycarbonates by copolymerization with CO_2.[19]

TBHP was chosen as the oxidant since the catalytic performance of oligo-/polymeric molybdenum oxide hybrid compounds for olefin epoxidation tends to be superior when using organic hydroperoxides as oxidants rather than, for example, H_2O_2.[3a,4a] Moreover, TBHP possesses relatively small molecular dimensions, which is important to avoid steric constraints, since the reaction mechanism typically involves coordination of the organic hydroperoxide to the metal center to give the active oxidizing species responsible for the oxygen transfer reaction to the olefin.[20] BTF and DCE were chosen as cosolvents since they (i) fully dissolve the reagents, (ii) are noncoordinating, thereby avoiding competition between the solvent and the reagents for coordination sites,[4b,21] and (iii) possess boiling points greater than 80 °C, avoiding high pressure and solvent evaporation during the catalytic reactions. DCE tends to enhance the catalytic epoxidation activity of oligo-/polymeric molybdenum oxide hybrid compounds with TBHP as oxidant.[4a,c] The hydrophobic nature of BTF is favorable for avoiding negative effects of moisture, for example, on product selectivity when the target epoxide product is more susceptible to acid-hydrolysis.[22]

The reaction of Ole with TBHP in the presence of **1**, at 55 °C, gave OleOx as the main product in high yields (77−83% at 24 h, Table 2). Without a catalyst, the Ole conversion was negligible. The rate of formation of OleOx was comparable for the two cosolvents (Figure 7A). On the other hand, while for BTF the OleOx selectivity was 100% at high conversions, for DCE a slight decrease in product selectivity was observed at comparably high conversions, with the concomitant formation of methyl 9,10-dihydroxystearate (OleDiol) as byproduct (4% OleDiol yield at 87% conversion, Table 2). The outstanding epoxide selectivity with BTF is possibly related to the high hydrophobicity of this solvent, thereby avoiding water in the reaction system. Increasing the reaction temperature from 55 to 75 °C enhanced the reaction rate (from ca. 42% to 89−93% conversion at 6 h reaction, using DCE or BTF, Table 2) without significantly affecting the dependence of OleOx yields on Ole conversion (Figure 7B). The reaction of Ole at 75 °C was complete within 24 h, giving an excellent OleOx yield of 98% with BTF as cosolvent (Table 2).

In the epoxidation of Lim at 55 °C, LimOx was obtained as the main reaction product in similar yields for the two organic cosolvents (ca. 85% at 24 h reaction, Table 3). In the temperature range of 55−75 °C, regioselectivity was very high toward the epoxidation of the endocyclic C=C bond. At Lim conversions greater than ca. 90%, the LimOx yield decreased slightly with concomitant increase in 1,2:8,9-diepoxy-*p*-menthane (LimDiOx) yield (3−7% yield) (Figure 8B), suggesting that LimOx is an intermediate in the formation of LimDiOx.

Table 2. Methyl Oleate Epoxidation with TBHP in the Presence of Molybdenum Compounds Possessing (Bi)pyridine Ligands

(pre)catalyst	T/°C	solvent	conv (%)[a]	OleOx yield (%)[a]	ref
1	55	DCE	43/87	43/83	this work
1	55	BTF	42/77	42/77	this work
$[Mo_8O_{22}(OH)_4$(di-*t*Bu-bipy)$_4]$	55	DCE	41/85	39/82	4b
$[Mo_8O_{22}(OH)_4$(di-*t*Bu-bipy)$_4]$	55	BTF	28/94	28/92	4b
1	75	DCE	89/100	85/95	this work
$[Mo(CO)_3I_2$(2,2′-bipy)$]$	75	DCE	47/72	~39/61	23
$[Mo(CO)_3I_2$(di-*t*Bu-bipy)$]$	75	DCE	65/78	58/71	23
$[Mo(CO)_3I_2(py)_2]$	75	DCE	16/25	~11/16	23
$[Mo(CO)_3I_2$(*t*Bu-py)$_2]$	75	DCE	23/37	~16/23	23
$[MoO_3$(2,2′-bipy)$]$	75	DCE	82/99	81//99	23
$[Mo_8O_{24}$(di-*t*Bu-bipy)$_4]$	75	DCE	100/100	≥99/≥99	23
$(C_5H_5NH)_4[Mo_8O_{26}]$	75	DCE	100/100	≥99/≥99	23
$[(CH_3)_3CC_5H_4NH]_4[Mo_8O_{26}]$	75	DCE	100/100	≥99/≥99	23
1	75	BTF	93/100	91/98	this work
1	75	[bmim]NTf_2	60/79 (−/74)[b]	60/76 (−/73)[b]	this work
1	75	[bmpy]BF_4	17/52	17/52	this work
1	75	[bmim]BF_4	23/50	23/50	this work
$[MoO_3$(2,2′-bipy)$]$	75	[bmim]BF_4	65/89	62/86	23

[a]Olefin conversion and epoxide yield at 6 h/24 h reaction using initial molar ratios Mo/olefin/TBHP = 1:103:160. [b]Values in parentheses are for a second catalytic batch run.

dx.doi.org/10.1021/ic400248m | *Inorg. Chem.* 2013, 52, 4618−4628

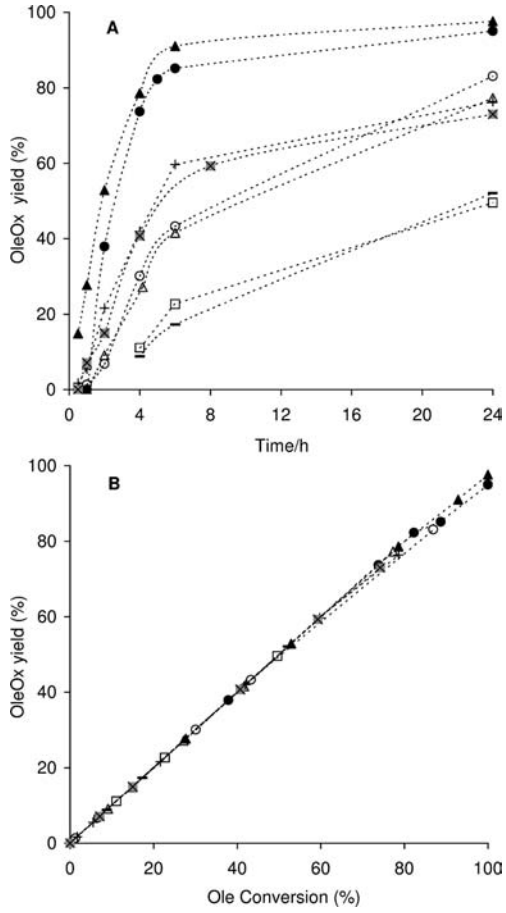

Figure 7. Dependence of OleOx yield on reaction time (A) or on Ole conversion (B) for the reaction of methyl oleate with TBHP in the presence of **1**: Ole/BTF/55 °C (Δ), Ole/BTF/75 °C (▲), Ole/DCE/55 °C (○), Ole/DCE/75 °C (●), Ole/[bmim]BF_4/75 °C (□), Ole/[bmpy]BF_4/75 °C (−), Ole/[bmim]NTf_2/75 °C/run1 (+), Ole/[bmim]NTf_2/75 °C/run 2 (×). The dashed lines are visual guides.

Table 3. DL-Limonene Epoxidation with TBHP in the Presence of 1 at 55 or 75 °C

reaction temp (°C)	solvent	conv (%)[a]	LimOx yield (%)[a]
55	DCE	65/90	61/84
	BTF	67/94	64/86
75	DCE	95/100	89/74
	BTF	95/100	86/76
	[bmim]NTf_2	74/76 (76/79)[b]	67/61 (66/64)[b]
	[bmim]BF_4	52/72	47/65

[a]Olefin conversion and epoxide yield at 6 h/24 h of reaction using initial molar ratios Mo/olefin/TBHP = 1:103:160. [b]Values in parentheses are for a second catalytic batch run.

Tables 2 and 4 compare the catalytic results for **1** with those reported for mono-/polynuclear molybdenum compounds possessing (bi)pyridine-type mono-/bidentate ligands, tested as (pre)catalysts for the same reactions under similar conditions. For Ole epoxidation, the catalytic results for **1** are in the midrange of those reported in the literature, while, for Lim epoxidation, **1** leads to comparable or even better results in terms of epoxide yield at 24 h.

For both substrates and both cosolvents, an initial induction period was observed at 55 °C (ca. 1 h for Ole and 2 h for Lim). Increasing the reaction temperature from 55 to 75 °C increased the initial reaction rates, and an induction period was only observed for DCE (Figures 7 and 8). These results may be explained by the fact that BTF better solubilizes the metal

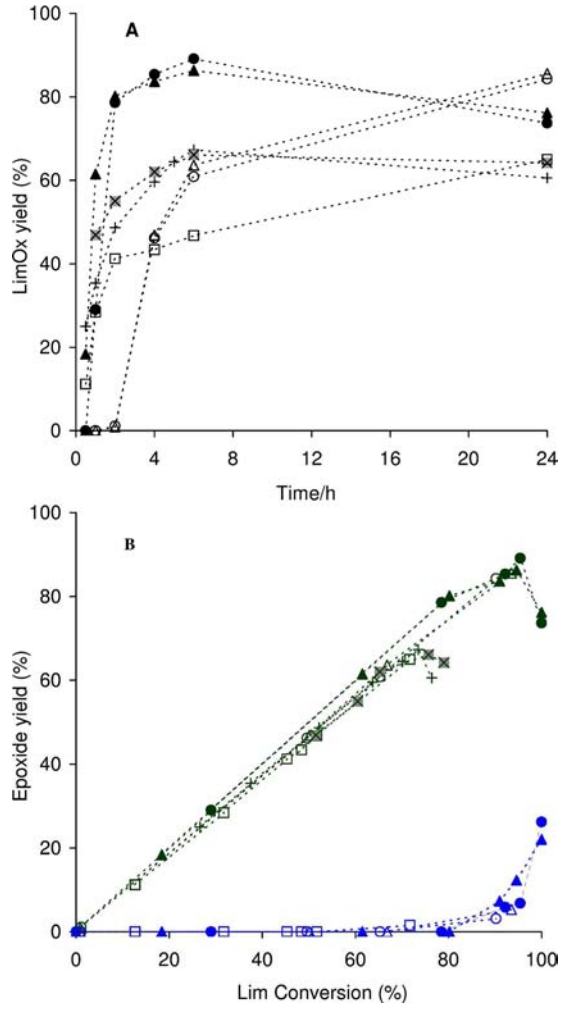

Figure 8. Dependence of LimOx yield on reaction time (A), and of LimOx yield (green symbols) and LimDiOx (blue symbols) on Lim conversion (B) for the reaction of DL-limonene with TBHP in the presence of **1**: Lim/BTF/55 °C (Δ), Lim/BTF/75 °C (▲), Lim/DCE/55 °C (○), Lim/DCE/75 °C (●), Lim/[bmim]BF_4/75 °C (□), Lim/[bmim]NTf_2/75 °C/run1 (+) and Lim/[bmim]NTf_2/75 °C/run 2 (×). The dashed lines are visual guides.

Table 4. DL-Limonene Epoxidation with TBHP at 55 °C in the Presence of Molybdenum Compounds Possessing Bipyridine-Type Ligands

(pre)catalyst	solvent	conv (%)[a]	LimOx yield (%)[a]	molar ratio LimOx/LimDiOx	ref
1	BTF	94	86	16[b]	this work
1	DCE	90	84	31[b]	this work
$[Mo_2O_6(L)_2]$[c]		99	71	3[d]	24
$[Mo_8O_{22}(OH)_4(L)_4]$[c]	DCE	96	81	10[e]	4b
$[Mo_8O_{22}(OH)_4(L)_4]$[c]	BTF	98	76	4[b]	4b

[a]Olefin conversion and epoxide yield at 24 h of reaction performed with initial molar ratio Mo/olefin/TBHP = 1:103:160. [b]No LimDiol was formed. [c]L = 4,4′-di-*tert*-butyl-2,2′-bipyridine. [d]LimDiol was formed in 3% yield. [e]LimDiol was formed in 5% yield.

dx.doi.org/10.1021/ic400248m | *Inorg. Chem.* 2013, 52, 4618−4628

species (the reaction mixtures with the organic cosolvents were always biphasic solid−liquid). Such an hypothesis assumes that the catalytic reaction takes place in the homogeneous phase, which was confirmed by the CatFilt test (details given in the Experimental Section) for **1**/Ole/TBHP/BTF/75 °C. A ΔFilt/Δcat ratio equal to 1 was obtained for this system, suggesting that the catalytic reaction is homogeneous in nature. A 4-fold decrease in the initial mass of **1**, using BTF at 75 °C, led to a slower reaction of Ole, with OleOx obtained as the only product in 65%/92% yield at 6 h/24 h; under these conditions, the reaction mixture was biphasic solid−liquid. The dependence of the reaction rate on the initial amount of catalyst was surprising, since the catalytic reaction takes place in the homogeneous phase and **1** was never fully dissolved in the reaction medium (i.e., the reaction mixture was apparently saturated with metal compound). Possibly, the initial rate of dissolution of the metal species in the liquid medium is rate-limiting to the overall reaction process. Similar effects have been reported for molybdenum-based epoxidation catalysts in the model reaction of *cis*-cyclooctene.[21b]

As discussed above, compound **1** and $[MoO_3(2,2'\text{-bipy})]$ are structurally related in that both comprise 1D organic−inorganic hybrid polymers, $_\infty^1[MoO_3(L)]^{n-}$ (n = 0, 1), formed by corner-sharing distorted $\{MoO_4N_2\}$ octahedra. Hence, a deeper comparison of their catalytic behaviors is appropriate. For the epoxidation of Ole at 75 °C using DCE as cosolvent, the OleOx yields at 6/24 h are comparable for both compounds (85/95% for **1** and 81/99% for $[MoO_3(2,2'\text{-bipy})]$, Table 2). Under these conditions, the reaction mixtures are always biphasic solid−liquid and the catalytic reactions are homogeneous in nature; that is, both compounds act as a source of active soluble species. A notable difference between the catalytic behaviors at 75 °C for the two compounds concerns the presence of an induction period for **1**, while no such period was observed for $[MoO_3(2,2'\text{-bipy})]$.[23] For $[MoO_3(2,2'\text{-bipy})]$, the powder XRD pattern and ATR FT-IR spectrum of the recovered solid matched those for the as-synthesized compound. For **1**, the attenuated total reflectance (ATR) FT-IR spectra of the as-synthesized and recovered solid were similar in the range 700−1400 cm^{-1}, and toward lower wavenumbers, some differences were evident, notably the appearance of a very broad absorption centered at ca. 600 cm^{-1} for the recovered solid (Figure S4). These differences may be related to differences observed in the powder XRD patterns for **1** and the corresponding recovered solid (Figure S4). The crystal structure (or packing) of **1** changes during the catalytic reaction, but the structural integrity of the 1D polymer seems to be retained. Possibly these structural modifications contribute to the induction period observed for **1**. We may speculate that these modifications involve a disruption of the strong hydrogen-bonding interactions involving the carboxylic acid groups of adjacent anionic $_\infty^1[(MoO_3)(Hbpdc)]^-$ chains, leading to a structurally less robust phase, fragments of which subsequently dissolve and catalyze the epoxidation reaction. The crystal packing in the hybrid material $[MoO_3(2,2'\text{-bipy})]$ does not contain such strong supramolecular contacts, which may partly explain why no induction period is observed.

One of the main drawbacks of homogeneous metal-based catalysts is the difficult catalyst recovery and reuse. Hence, in this work, ionic liquids (ILs) were explored as solvents instead of DCE or BTF in an attempt to facilitate catalyst recycling. The ILs $[bmim]BF_4$, $[bmim]NTf_2$, and $[bmpy]BF_4$ were chosen due to their commercial availability, relatively low price, and stability under the reaction conditions used. Indeed, $[bmim]BF_4$ and $[bmim]NTf_2$ have already been successfully used as cosolvents for the epoxidation of olefins in the presence of molybdenum-based homogeneous catalysts.[23,25] For the **1**/TBHP/IL/75 °C systems (without olefin) the "non-productive" decomposition of TBHP (into *tert*-butanol and molecular oxygen) was determined by iodometric titration and found to be less than 6% after 6 h. For the same systems with Ole but without catalyst, no reaction took place.

The dependence of OleOx yield on Ole conversion was similar for the organic and IL solvent systems examined in this work (Figure 7B). A comparison of the results for the three ILs shows that the formation of OleOx was faster for $[bmim]NTf_2$ (60%/76% yield at 60%/79% conversion reached at 6 h/24 h reaction, Table 2, Figure 7A). The BF_4^--containing ILs led to 50−52% OleOx yield (100% selectivity) at 24 h (Table 2, Figure 7A); these similar results for $[bmim]BF_4$ and $[bmpy]BF_4$ parallel those reported by Wang and co-workers for the epoxidation of fatty acid methyl esters in the presence of $[MoO(O_2)_2\cdot 2(8\text{-quinilinol})]$ as catalyst.[25b] The anion (rather than the cation) of the IL seems to play an important role, and the relatively high hydrophobicity and low viscosity of $[bmim]NTf_2$ may be favorable for the overall reaction process.[26] In contrast to that observed for the BF_4^--containing ILs, the reagents were completely dissolved in $[bmim]NTf_2$. Considering the good solubilization properties and relatively low viscosity of $[bmim]NTf_2$, mass transfer limitations may be less important. The recyclability of the catalyst/$[bmim]NTf_2$ system was investigated by carrying out a second 24 h batch run of the reaction of Ole at 75 °C, using the recovered catalyst/$[bmim]NTf_2$ mixture (please see the Experimental Section for details). The catalytic results were similar for the two consecutive runs, suggesting that the **1**/$[bmim]NTf_2$ system can be effectively recycled (Table 2, Figure 7). In parallel to that observed for Ole, the formation of LimOx from Lim was faster for $[bmim]NTf_2$ than for $[bmim]BF_4$, and similar catalytic results were obtained in the two consecutive 24 h batch runs using $[bmim]NTf_2$ as cosolvent (Figure 8A, Table 3).

CONCLUSIONS

Three molybdenum oxide/bipyridine hybrid materials containing the same type of one-dimensional polymer, $_\infty^1[MoO_3(bipy)]$, formed by corner-sharing distorted $\{MoO_4N_2\}$ octahedra, are now known, namely $[MoO_3(2,2'\text{-bipy})]$,[2a,3a] $\{[MoO_3(2,2'\text{-bipy})][MoO_3(H_2O)]\}_n$,[4a] and (in this work) (DMA)$[MoO_3(Hbpdc)]\cdot H_2O$ (**1**). The alignment of the organic ligands is different for all these materials. Whereas in $\{[MoO_3(2,2'\text{-bipy})][MoO_3(H_2O)]\}_n$ the bipy ligands of the $_\infty^1[MoO_3(2,2'\text{-bipy})]$ polymer are perfectly aligned so as to minimize steric repulsion with the adjacent $_\infty^1[MoO_3(H_2O)]$, in $[MoO_3(2,2'\text{-bipy})]$ the bipy rings fan out along the chains so as to minimize steric repulsion between adjacent organic ligands. In compound **1** the mutual rotation of the bipy ligands is restricted to a lower amount due to the strong and highly directional O−H···O hydrogen bonds involving the carboxylic acid groups.

When the materials mentioned above are employed in catalytic olefin epoxidation with *tert*-butylhydroperoxide as oxidant, the reactions are usually at least partially homogeneous in nature (especially when a polar cosolvent is used); that is, the materials act as a source of active soluble species. For

dx.doi.org/10.1021/ic400248m | Inorg. Chem. 2013, 52, 4618−4628

compound **1**, the reactions of methyl oleate (Ole) and DL-limonene (Lim) give methyl 9,10-epoxystearate and 1,2-epoxy-*p*-menth-8-ene as the main products in yields of up to 98% and 89%, respectively (24 h, 75 °C). For Ole epoxidation, the catalytic results for **1** are in the midrange of those reported for other mono-/polynuclear molybdenum compounds possessing (bi)pyridine-type mono-/bidentate ligands, while, for Lim epoxidation, **1** leads to comparable or even better results in terms of epoxide yield. We have further shown that the catalyst recycling issue can be successfully addressed by using an ionic liquid as cosolvent with solvent extraction of the target epoxide products between recycles.

An attractive goal with molybdenum oxide/bipyridine hybrid materials is heterogeneous catalysis, especially since the 1D inorganic−organic chains present in the three materials mentioned above can be considered as polymeric versions of monomeric $[MoO_2(OR)_2(bipy)]$ complexes, which are well-known as effective homogeneous olefin epoxidation catalysts. As previously demonstrated for $\{[MoO_3(2,2'\text{-bipy})][MoO_3(H_2O)]\}_n$,[4a] the catalytic reaction may take place heterogeneously by adjusting the reaction conditions (albeit with relatively low activity, at least partly due to the low amount of accessible active sites). There is a need to develop porous molybdenum oxide/organic hybrid materials with improved active site accessibility and that function as heterogeneous catalysts. As supported by the present work, the introduction of substituents on the organic ligands is one approach to expand the structural complexity of these systems, and with further work, this may lead to the preparation of supramolecular frameworks with the desired properties.

■ ASSOCIATED CONTENT

Supporting Information

Detailed description of X-ray diffraction studies, Figures S1−S4, Tables S1−S2, and crystallographic information file (CIF). This material is available free of charge via the Internet at http://pubs.acs.org.

■ AUTHOR INFORMATION

Corresponding Author

*E-mail: filipe.paz@ua.pt (F.A.A.P.), igoncalves@ua.pt (I.S.G.).

Notes

The authors declare no competing financial interest.

■ ACKNOWLEDGMENTS

We are grateful to the Fundação para a Ciência e a Tecnologia (FCT), QREN, Fundo Europeu de Desenvolvimento Regional (FEDER), COMPETE, and the European Union for funding (R&D Project No. PDTC/QUI-QUI/098098/2008, FCOMP-01-0124-FEDER-010785). The Associate Laboratory CICECO (Pest-C/CTM/LA0011/2011) is acknowledged for continued support and funding. We thank the FCT and the European Union for a postdoctoral grant to P.N. (SFRH/BPD/73540/2010), cofunded by MCTES and the European Social Fund through the program POPH of QREN, and for a Ph.D. grant to T.R.A. (SFRH/BD/64224/2009). We further wish to acknowledge the European Synchrotron Radiation Facility (Grenoble, France) for granting access time to the ID31 beamline under the CH-3692 and CH-3702 research proposals.

■ REFERENCES

(1) (a) Hagrman, P. J.; Hagrman, D.; Zubieta, J. *Angew. Chem., Int. Ed.* **1999**, *38*, 2638. (b) Hagrman, D.; Hagrman, P. J.; Zubieta, J. *Comments Inorg. Chem.* **1999**, *21*, 225. (c) Han, W.; Yuan, P.; Fan, Y.; Liu, H.; Bao, X. *J. Mater. Chem.* **2012**, *22*, 12121. (d) Han, W.; Yuan, P.; Fan, Y.; Shi, G.; Liu, H.; Bai, D.; Bao, X. *J. Mater. Chem.* **2012**, *22*, 25340.

(2) (a) Zapf, P. J.; Haushalter, R. C.; Zubieta, J. *Chem. Mater.* **1997**, *9*, 2019. (b) Kim, J.; Lim, W. T.; Koo, B. K. *Inorg. Chim. Acta* **2007**, *360*, 2187. (c) Lu, Y.; Wang, E.; Yuan, M.; Li, Y.; Hu, C. *J. Mol. Struct.* **2003**, *649*, 191. (d) Hagrman, P. J.; LaDuca, R. L., Jr.; Koo, H.-J.; Rarig, R., Jr.; Haushalter, R. C.; Whangbo, M.-H.; Zubieta, J. *Inorg. Chem.* **2000**, *39*, 4311. (e) Cui, C.-P.; Dai, J.-C.; Du, W.-X.; Fu, Z.-Y.; Hu, S.-M.; Wu, L.-M.; Wu, X.-T. *Polyhedron* **2002**, *21*, 175. (f) Niu, J.; Wang, Z.; Wang, J. *Inorg. Chem. Commun.* **2004**, *7*, 556. (g) Xu, Y.; Lu, J. *Inorg. Chim. Acta* **1999**, *295*, 222. (h) Zapf, P. J.; LaDuca, R. L., Jr.; Rarig, R. S., Jr.; Johnson, K. M., III; Zubieta, J. *Inorg. Chem.* **1998**, *37*, 3411. (i) LaDuca, R. L., Jr.; Rarig, R. S., Jr.; Zapf, P. J.; Zubieta, J. *Inorg. Chim. Acta* **1999**, *292*, 131. (j) Zhou, Y.; Zhang, L.; Fun, H.-K.; You, X. *Inorg. Chem. Commun.* **2000**, *3*, 114. (k) Li, D.; Liu, Y.; Wei, P.; Hu, B.; Zhang, X. *Acta Crystallogr., Sect. E: Struct. Rep. Online* **2009**, *E65*, m1074. (l) Xu, Y.; Lu, J.; Goh, N. K. *J. Mater. Chem.* **1999**, *9*, 1599. (m) Rarig, R. S., Jr.; Zubieta, J. *Inorg. Chim. Acta* **2001**, *312*, 188. (n) Chuang, J.; Ouellette, W.; Zubieta, J. *Inorg. Chim. Acta* **2008**, *361*, 2357. (o) Lysenko, A. B.; Senchyk, G. A.; Lincke, J.; Lässig, D.; Fokin, A. A.; Butova, E. D.; Schreiner, P. R.; Krautscheid, H.; Domasevitch, K. V. *Dalton Trans.* **2010**, *39*, 4223. (p) Hagrman, D.; Zubieta, C.; Rose, D. J.; Zubieta, J.; Haushalter, R. C. *Angew. Chem., Int. Ed. Engl.* **1997**, *36*, 873. (q) Zapf, P. J.; Warren, C. J.; Haushalter, R. C.; Zubieta, J. *Chem. Commun.* **1997**, 1543. (r) Hagrman, D.; Zapf, P. J.; Zubieta, J. *Chem. Commun.* **1998**, 1283. (s) Hagrman, D.; Sangregorio, C.; O'Connor, C. J.; Zubieta, J. *J. Chem. Soc., Dalton Trans.* **1998**, 3707. (t) Hagrman, P. J.; Zubieta, J. *Inorg. Chem.* **2000**, *39*, 5218. (u) Rarig, R. S., Jr.; Lam, R.; Zavalij, P. Y.; Ngala, J. K.; LaDuca, R. L., Jr.; Greedan, J. E.; Zubieta, J. *Inorg. Chem.* **2002**, *41*, 2124. (v) Kong, Z.; Weng, L.; Tan, D.; He, H.; Zhang, B.; Kong, J.; Yue, B. *Inorg. Chem.* **2004**, *43*, 5676. (w) Coué, V.; Dessapt, R.; Bujoli-Doeuff, M.; Evain, M.; Jobic, S. *Inorg. Chem.* **2007**, *46*, 2824. (x) Yang, M.-X.; Chen, L.-J.; Lin, S.; Chen, X.-H.; Huang, H. *Dalton Trans.* **2011**, *40*, 1866.

(3) (a) Amarante, T. R.; Neves, P.; Coelho, A. C.; Gago, S.; Valente, A. A.; Paz, F. A. A.; Pillinger, M.; Gonçalves, I. S. *Organometallics* **2010**, *29*, 883. (b) Neves, P.; Amarante, T. R.; Gomes, A. C.; Coelho, A. C.; Gago, S.; Pillinger, M.; Gonçalves, I. S.; Silva, C. M.; Valente, A. A. *Appl. Catal. A: Gen.* **2011**, *395*, 71.

(4) (a) Abrantes, M.; Amarante, T. R.; Antunes, M. M.; Gago, S.; Paz, F. A. A.; Margiolaki, I.; Rodrigues, A. E.; Pillinger, M.; Valente, A. A.; Gonçalves, I. S. *Inorg. Chem.* **2010**, *49*, 6865. (b) Amarante, T. R.; Neves, P.; Tomé, C.; Abrantes, M.; Valente, A. A.; Paz, F. A. A.; Pillinger, M.; Gonçalves, I. S. *Inorg. Chem.* **2012**, *51*, 3666. (c) Figueiredo, S.; Gomes, A. C.; Neves, P.; Amarante, T. R.; Paz, F. A. A.; Soares, R.; Lopes, A. D.; Valente, A. A.; Pillinger, M.; Gonçalves, I. S. *Inorg. Chem.* **2012**, *51*, 8629.

(5) Abrantes, M.; Gonçalves, I. S.; Pillinger, M.; Vurchio, C.; Cordero, F. M.; Brandi, A. *Tetrahedron Lett.* **2011**, *52*, 7079.

(6) (a) Schoknecht, B.; Kempe, R. *Z. Anorg. Allg. Chem.* **2004**, *630*, 1377. (b) Szeto, K. C.; Prestipino, C.; Lamberti, C.; Zecchina, A.; Bordiga, S.; Bjørgen, M.; Tilset, M.; Lillerud, K. P. *Chem. Mater.* **2007**, *19*, 211. (c) Szeto, K. C.; Kongshaug, K. O.; Jakobsen, S.; Tilset, M.; Lillerud, K. P. *Dalton Trans.* **2008**, 2054. (d) Huh, S.; Jung, S.; Kim, Y.; Kim, S.-J.; Park, S. *Dalton Trans.* **2010**, *39*, 1261. (e) Blake, A. J.; Champness, N. R.; Easun, T. L.; Allan, D. R.; Nowell, H.; George, M. W.; Jia, J.; Sun, X.-Z. *Nat. Chem.* **2010**, *2*, 688. (f) Bloch, E. D.; Britt, D.; Lee, C.; Doonan, C. J.; Uribe-Romo, F. J.; Furukawa, H.; Long, J. R.; Yaghi, O. M. *J. Am. Chem. Soc.* **2010**, *132*, 14382. (g) Long, J.; Wang, L.; Gao, X.; Bai, C.; Jiang, H.; Li, Y. *Chem. Commun.* **2012**, *48*, 12109. (h) Shen, L.; Gray, D.; Masel, R. I.; Girolami, G. S. *CrystEngComm* **2012**, *14*, 5145. (i) Gustafsson, M.; Su, J.; Yue, H.; Yao, Q.; Zou, X. *Cryst. Growth Des.* **2012**, *12*, 3243.

(7) Brandenburg, K. *DIAMOND*, Version 3.2f; Crystal Impact GbR: Bonn, Germany, 1997−2010.
(8) Atencio, R.; Briceño, A.; Silva, P.; Rodríguez, J. A.; Hanson, J. C. *New J. Chem.* **2007**, *31*, 33.
(9) (a) Bator, G.; Baran, J.; Jakubas, R.; Sobczyk, L. *J. Mol. Struct.* **1998**, *450*, 89. (b) Wojtaś, M.; Bator, G.; Baran, J. *Vib. Spectrosc.* **2003**, *33*, 143. (c) Shi, F.-N.; Cunha-Silva, L.; Trindade, T.; Paz, F A. A.; Rocha, J. *Cryst. Growth Des.* **2009**, *9*, 2098.
(10) (a) Burrows, A. D.; Cassar, K.; Friend, R. M. W.; Mahon, M. F.; Rigby, S. P.; Warren, J. E. *CrystEngComm* **2005**, *7*, 548. (b) Clausen, H. F.; Poulsen, R. D.; Bond, A. D.; Chevallier, M.-A. S.; Iversen, B. B. *J. Solid State Chem.* **2005**, *178*, 3342. (c) Ganesan, S. V.; Lightfoot, P.; Natarajan, S. *Solid State Sci.* **2004**, *6*, 757.
(11) Li, Y. G.; Dai, L. M.; Wang, Y. H.; Wang, X. L.; Wang, E. B.; Su, Z. M.; Xu, L. *Chem. Commun.* **2007**, 2593.
(12) Dai, L. M.; You, W. S.; Li, Y. G.; Wang, E. B.; Qi, L. J.; Tang, J.; Bai, X. L. *Inorg. Chem. Commun.* **2010**, *13*, 421.
(13) Allen, F. H. *Acta Crystallogr., Sect. B: Struct. Sci.* **2002**, *58*, 380.
(14) Allen, F. H.; Motherwell, W. D. S. *Acta Crystallogr., Sect. B: Struct. Sci.* **2002**, *58*, 407.
(15) Bernstein, J.; Davis, R. E.; Shimoni, L.; Chang, N. L. *Angew. Chem., Int. Ed. Engl.* **1995**, *34*, 1555.
(16) Lligadas, G.; Ronda, J. C.; Galia, M.; Biermann, U.; Metzger, J. O. *J. Polym. Sci., Part A: Polym. Chem.* **2006**, *44*, 634.
(17) Doll, K. M.; Erhan, S. Z. *J. Agric. Food Chem.* **2005**, *53*, 9608.
(18) Biswas, A.; Sharma, B. K.; Willett, J. L.; Advaryu, A.; Erhan, S. Z.; Cheng, H. N. *J. Agric. Food Chem.* **2008**, *56*, 5611.
(19) (a) Byrne, C. M.; Allen, S. D.; Lobkovsky, E. B.; Coates, G. W. *J. Am. Chem. Soc.* **2004**, *126*, 11404. (b) Corma, A.; Iborra, S.; Velty, A. *Chem. Rev.* **2007**, *107*, 2411.
(20) (a) Veiros, L. F.; Prazeres, A.; Costa, P. J.; Romão, C. C.; Kühn, F. E.; Calhorda, M. J. *Dalton Trans.* **2006**, 1383. (b) Kühn, F. E.; Groarke, M.; Bencze, E.; Herdtweck, E.; Prazeres, A.; Santos, A. M.; Calhorda, M. J.; Romão, C. C.; Gonçalves, I. S.; Lopes, A. D.; Pillinger, M. *Chem.—Eur. J.* **2002**, *8*, 2370.
(21) (a) Gago, S.; Neves, P.; Monteiro, B.; Pessêgo, M.; Lopes, A. D.; Valente, A. A.; Paz, F. A. A.; Pillinger, M.; Moreira, J.; Silva, C. M.; Gonçalves, I. S. *Eur. J. Inorg. Chem.* **2009**, 4528. (b) Gomes, A. C.; Neves, P.; Figueiredo, S.; Fernandes, J. A.; Valente, A. A.; Paz, F. A. A.; Pillinger, M.; Lopes, A. D.; Gonçalves, I. S. *J. Mol. Catal. A: Chem.* **2013**, *370*, 64.
(22) Maul, J. J.; Ostrowski, P. J.; Ublacker, G. A.; Linclau, B.; Curran, D. P. In *Modern Solvents in Organic Synthesis*; Knochel, P., Ed.; Springer: Berlin Heidelberg: 1999; Vol. *206*, p 79.
(23) Gamelas, C. A.; Neves, P.; Gomes, A. C.; Valente, A. A.; Romão, C. C.; Gonçalves, I. S.; Pillinger, M. *Catal. Lett.* **2012**, *142*, 1218.
(24) Amarante, T. R.; Neves, P.; Paz, F. A. A.; Pillinger, M.; Valente, A. A.; Gonçalves, I. S. *Inorg. Chem. Commun.* **2012**, *20*, 147.
(25) (a) Brito, J. A.; Ladeira, S.; Teuma, E.; Royo, B.; Gomez, M. *Appl. Catal. A: Gen.* **2011**, *398*, 88. (b) Cai, S.-F.; Wang, L.-S.; Fan, C.-L. *Molecules* **2009**, *14*, 2935. (c) Betz, D.; Raith, A.; Cokoja, M.; Kühn, F. E. *ChemSusChem* **2010**, *3*, 559. (d) Valente, A. A.; Petrovski, Z.; Branco, L. C.; Afonso, C. A. M.; Pillinger, M.; Lopes, A. D.; Romão, C. C.; Nunes, C. D.; Gonçalves, I. S. *J. Mol. Catal. A: Chem.* **2004**, *218*, 5. (e) Günyar, A.; Betz, D.; Drees, M.; Herdtweck, E.; Kühn, F. E. *J. Mol. Catal. A: Chem.* **2010**, *331*, 117. (f) Betz, D.; Herrmann, W. A.; Kühn, F. E. *J. Organomet. Chem.* **2009**, *694*, 3320. (g) Bibal, C.; Daran, J. C.; Deroover, S.; Poli, R. *Polyhedron* **2010**, *29*, 639. (h) Kühn, F. E.; Zhao, J.; Abrantes, M.; Sun, W.; Afonso, C. A. M.; Branco, L. C.; Gonçalves, I. S.; Pillinger, M.; Romão, C. C. *Tetrahedron Lett.* **2005**, *46*, 47.
(26) Huddleston, J. G.; Visser, A. E.; Reichert, W. M.; Willauer, H. D.; Broker, G. A.; Rogers, R. D. *Green Chem.* **2001**, *3*, 156.